Research Square

Preprints are preliminary reports that have not undergone peer review.
They should not be considered conclusive, used to inform clinical practice,
or referenced by the media as validated information.

Quantitative finite-patch obstructions to null controllability of a rotationally damped shear beam

Assane Lo

assanelo@uowdubai.ac.ae

University of Wollongong in Dubai

Umar Asghar

University of Wollongong in Dubai

Ciara O'Driscoll

University of Wollongong in Dubai

Majid Munawar

University of Wollongong in Dubai

Research Article

Keywords: Shear beam, null controllability, observability, piezoelectric patch, spectral asymptotics, Diophantine approximation

Posted Date: September 23rd, 2026

DOI: https://doi.org/10.21203/rs.3.rs-10886247/v1

License: This work is licensed under a Creative Commons Attribution 4.0 International License.
Read Full License

Additional Declarations: No competing interests reported.

Quantitative finite-patch obstructions to null controllability of a rotationally damped shear beam

Assane Lo[1*], Umar Asghar[1], Ciara O'Driscoll[1], Majid Munawar[1]

[1*]University of Wollongong in Dubai, Dubai, United Arab Emirates.

*Corresponding author(s). E-mail(s): assanelo@uowdubai.ac.ae;

Abstract

We study null controllability of a rotationally damped shear beam without rotary inertia when the controls are a fixed finite family of piezoelectric patches represented by endpoint moments. A spatially uniform rotation control is also allowed. The associated dynamics form a mixed hyperbolic–parabolic semigroup. We first identify an invariant rotation mean and show precisely how the uniform channel removes this scalar obstruction. On the zero-mean energy space, we derive the final-state observability criterion, the modal characteristic polynomial, and a weakly damped wave branch whose real parts are of order $-n^{-2}$. Simultaneous Diophantine approximation of the patch lengths yields normalized adjoint modes for which all finite-patch observations vanish asymptotically while the terminal energy remains bounded away from zero. Consequently, no finite placement of these patches gives L^2-null controllability in the natural energy space at any positive time, even after the mean mode is made controllable. Quantitatively, for a Galerkin truncation with K modes and M displacement patches, the best observability constants grow at least as $K^{2/M}$ along a subsequence, and the corresponding least-control norms grow at least as $K^{1/M}$. A Fourier–Galerkin implicit-midpoint scheme satisfies an exact discrete energy-dissipation identity. Numerical experiments verify the spectral asymptotics and illustrate the resulting growth of truncated observability costs.

Keywords: Shear beam, null controllability, observability, piezoelectric patch, spectral asymptotics, Diophantine approximation

MSC Classification: 93B05 , 93C20 , 35B35 , 74K10

1 Introduction

Piezoelectric patches are commonly represented in one-dimensional beam models by equal and opposite moments concentrated at the two patch endpoints. This leads to spatial inputs of the form $\partial_x(\delta_\mu - \delta_\xi)$, whose dual observation is a difference of pointwise slopes. For Euler–Bernoulli and Rayleigh beams, the resulting controllability properties depend strongly on the actuator location, the control regularity, and the spectral density; see, for example, [2, 6, 13].

The shear beam studied here has a different structure. The transverse displacement equation is hyperbolic, whereas the absence of rotary inertia makes the rotation equation parabolic–elliptic. Ramos et al. [12] prove well-posedness and lack of exponential stability when damping acts on the rotation. Recent work identifies the associated sharp polynomial decay [11, 15]. These facts make it essential to distinguish exact controllability from null controllability and to use the final-state observability criterion appropriate to a non-invertible semigroup.

For laminated Timoshenko structures with a separate interfacial-slip variable, Lo and Tatar established two complementary positive stabilization results. A memory term acting on the effective rotation yields exponential energy decay under explicit kernel, equal-wave-speed, and parameter conditions [9]. They subsequently proved exponential decay for a related slip model with transverse friction, and also for a viscoelastic model when the relaxation mass is sufficiently small [10]. These results show that distributed friction or memory can suppress the troublesome structural modes. They do not, however, imply controllability by finitely many localized patches: the models have a third slip variable, different boundary conditions and damping operators, and the conclusions concern free-energy decay rather than a uniform lower bound for an adjoint observation. This distinction is central to the actuator limitation proved below.

The contributions of this paper are fivefold.

(i) We prove that the mean rotation is unaffected by every endpoint-moment patch and show that a single uniform rotation input controls this scalar mode.
(ii) On the invariant zero-mean space, we derive the correct modal system, characteristic polynomial, and weakly damped wave branch.
(iii) We combine this branch with simultaneous approximation of all patch lengths to disprove energy observability for an arbitrary finite number of patches, independently of their placement and of the control time.
(iv) We quantify the defect by a subsequential lower bound on the observability and least-control costs of spectral Galerkin models.
(v) We prove a discrete energy identity for an implicit-midpoint Fourier–Galerkin scheme and use reproducible numerical experiments to illustrate both the weak damping and the cost-growth mechanism.

This conclusion does not exclude controllability in a weighted or smoother state space. The Rayleigh-beam results in [2] and the recent analysis of wave–heat cascades in [7] show why mixed hyperbolic–parabolic systems with concentrated actuation naturally lead to control spaces that depend on modal coefficients. Our result instead

locates the sharp obstruction to natural-energy null controllability for the present actuator class.

2 The controlled shear-beam model

Let $L > 0$ and let $\rho, \lambda, \kappa, \gamma$ be positive constants. Fix integers $M, N \geq 0$. For $0 < x < L$ and $t > 0$, the transverse displacement $w = w(x,t)$ and rotation $\varphi = \varphi(x,t)$ satisfy

$$\begin{cases} \rho w_{tt} - \kappa(w_x + \varphi)_x = \displaystyle\sum_{j=1}^{M} u_j(t)\, \partial_x(\delta_{\mu_j} - \delta_{\xi_j}), \\ -\lambda\varphi_{xx} + \kappa(w_x + \varphi) + \gamma\varphi_t = h(t) + \displaystyle\sum_{k=1}^{N} v_k(t)\, \partial_x(\delta_{\beta_k} - \delta_{\alpha_k}), \end{cases} \tag{1}$$

with

$$w(0,t) = w(L,t) = 0, \qquad \varphi_x(0,t) = \varphi_x(L,t) = 0. \tag{2}$$

Here $0 < \xi_j < \mu_j < L$, $0 < \alpha_k < \beta_k < L$, and all scalar controls belong to $L^2(0,T)$. The uniform channel h is optional: setting $h = 0$ recovers pure patch actuation. The endpoint model is consistent with the usual equal-and-opposite moment idealization [5, 13]. Unlike the laminated systems in [9, 10], model (1) has no interfacial-slip state and no hereditary damping term. Accordingly, their exponential-stability estimates cannot be inserted into the present semigroup or used in place of the observability analysis.

For smooth unforced solutions, the natural energy is

$$E(t) = \frac{1}{2}\left(\rho\,\|w_t(t)\|_{L^2}^2 + \lambda\,\|\varphi_x(t)\|_{L^2}^2 + \kappa\,\|w_x(t) + \varphi(t)\|_{L^2}^2\right), \tag{3}$$

and direct multiplication of the two equations by w_t and φ_t gives

$$E'(t) = -\gamma\,\|\varphi_t(t)\|_{L^2}^2 \leq 0. \tag{4}$$

The corresponding zero-mean energy space is

$$\begin{aligned} \mathcal{X}_* &:= H_0^1(0,L) \times L^2(0,L) \times H_*^1(0,L), \\ H_*^1(0,L) &:= \left\{ f \in H^1(0,L) : \int_0^L f\,\mathrm{d}x = 0 \right\}. \end{aligned} \tag{5}$$

equipped with the norm induced by twice the energy in (3). On H_*^1, this is equivalent to the standard product norm. Homogeneous well-posedness and contraction-semigroup formulations for this shear model are given in [11, 12]. For the singularly forced problem, solutions are understood by transposition whenever the finitely many slope observations below are L^2-admissible. If this admissibility fails, the usual L^2 control problem is not well posed; our non-controllability statement concerns every admissible realization.

Definition 2.1 System (1)–(2) is L^2-*null controllable at time* T *in a state space* X if, for every initial state in X, there are $h, u_1, \dots, u_M, v_1, \dots, v_N \in L^2(0,T)$ such that

$$w(\cdot,T) = w_t(\cdot,T) = \varphi(\cdot,T) = 0.$$

Because the damped shear semigroup is not a group, this property must not be identified with exact controllability to an arbitrary final state.

3 A finite-dimensional obstruction

The first obstruction is visible without spectral analysis.

Theorem 3.1 (Exact equation for the rotation mean) *Let* (w,φ) *be any transposition solution of* (1)–(2). *Then*

$$m(t) = e^{-\kappa t/\gamma} m(0) + \frac{L}{\gamma} \int_0^t e^{-\kappa(t-s)/\gamma} h(s)\,\mathrm{d}s, \qquad m(t) := \int_0^L \varphi(x,t)\,\mathrm{d}x. \tag{6}$$

Consequently, every endpoint-moment patch leaves the mean uncontrolled. If $h = 0$ *and* $m(0) \neq 0$, *null controllability on* $H_0^1(0,L) \times L^2(0,L) \times H^1(0,L)$ *fails at every finite time. If* h *is allowed, the scalar mean can be driven to zero at every* $T > 0$.

Proof We first argue for a smooth solution; the identity then passes to transposition solutions by density. Integrating the second equation of (1) over $(0,L)$ gives

$$\begin{aligned} -\lambda\big[\varphi_x(L,t) - \varphi_x(0,t)\big] + \kappa\big[w(L,t) - w(0,t)\big] + \kappa \int_0^L \varphi(x,t)\,\mathrm{d}x \\ + \gamma \frac{\mathrm{d}}{\mathrm{d}t} \int_0^L \varphi(x,t)\,\mathrm{d}x = Lh(t) + \sum_{k=1}^N v_k(t) \left\langle \partial_x(\delta_{\beta_k} - \delta_{\alpha_k}), 1 \right\rangle. \end{aligned}$$

The boundary conditions annihilate the first two brackets. Moreover, for any $0 < a < b < L$, the definition of the distributional derivative gives

$$\langle \partial_x(\delta_b - \delta_a), 1\rangle = -\langle \delta_b - \delta_a, (1)_x\rangle = 0.$$

Thus m satisfies in $\mathcal{D}'(0,T)$ the scalar equation $\gamma m' + \kappa m = Lh$. Since $h \in L^2(0,T)$, this equation has an absolutely continuous solution. Multiplication by the integrating factor $e^{\kappa t/\gamma}$ and integration from 0 to t give (6).

If $h = 0$, then $m(T) = e^{-\kappa T/\gamma} m(0)$, which is nonzero whenever $m(0) \neq 0$; no choice of patch controls can alter it. If h is allowed, the constant control

$$h(t) = -\frac{\kappa}{L} \frac{e^{-\kappa T/\gamma}}{1 - e^{-\kappa T/\gamma}} m(0), \qquad 0 < t < T,$$

belongs to $L^2(0,T)$. Substitution in (6) gives

$$m(T) = e^{-\kappa T/\gamma} m(0) - \frac{\kappa}{\gamma} \frac{e^{-\kappa T/\gamma}}{1 - e^{-\kappa T/\gamma}} m(0) \int_0^T e^{-\kappa(T-s)/\gamma}\,\mathrm{d}s = 0.$$

Finally, approximate transposition data and controls by smooth sequences. The mean functional is continuous on $H^1(0,L)$ and the scalar formula is stable under $L^2(0,T)$ convergence of h, so the identity remains valid in the stated solution class. □

For pure patch actuation the restriction to $H^1_*(0,L)$ is therefore necessary, not merely a device for applying Poincaré's inequality. The uniform channel removes this finite-dimensional obstruction, but Theorem 5.3 below shows that it does not remove the high-frequency one. An analogous mean-mode reduction is used for Neumann thermal variables in [3].

4 The correct adjoint criterion

We record the duality calculation because it fixes both the sign of the damping term and the terminal condition. Let (p,q) be smooth and satisfy the same spatial boundary conditions as (w,φ). Multiply the two equations in (1) by p and q, respectively, integrate over $(0,L)\times(0,T)$, and integrate twice in time in the w term and once in time in the φ term. The spatial terms are integrated by parts using $w=p=0$ and $\varphi_x = q_x = 0$ at $x=0,L$. The interior terms multiplying w and φ vanish precisely when

$$\begin{cases} \rho p_{tt} - \kappa(p_x+q)_x = 0, \\ -\lambda q_{xx} + \kappa(p_x+q) - \gamma q_t = 0, \end{cases} \tag{7}$$

with $p(0,t)=p(L,t)=0$ and $q_x(0,t)=q_x(L,t)=0$. One obtains the exact Lagrange identity

$$\begin{aligned} &\left[\int_0^L \big\{\rho(w_t p - w p_t) + \gamma\varphi q\big\}\,\mathrm{d}x\right]_{t=0}^{t=T} \\ &= \int_0^T \left[\sum_{j=1}^M u_j(t)\big(p_x(\xi_j,t) - p_x(\mu_j,t)\big) + h(t)\int_0^L q(x,t)\,\mathrm{d}x \right. \\ &\qquad \left. + \sum_{k=1}^N v_k(t)\big(q_x(\alpha_k,t) - q_x(\beta_k,t)\big)\right]\mathrm{d}t. \end{aligned} \tag{8}$$

For example,

$$\big\langle \partial_x(\delta_{\mu_j} - \delta_{\xi_j}), p\big\rangle = -p_x(\mu_j) + p_x(\xi_j),$$

which explains the order of the endpoints in (8). The data $(p(\cdot,T), p_t(\cdot,T), q(\cdot,T))$ are arbitrary. Imposing zero terminal data would make the adjoint identically zero and therefore could not test the reachability map.

With the time reversal $\tau = T-t$, $P(x,\tau) = p(x,T-\tau)$, and $Q(x,\tau) = q(x,T-\tau)$, system (7) becomes the homogeneous version of (1). The control/observation duality is

$$\begin{aligned} \mathcal{O}(P,Q)(\tau) = \Big(&\big(P_x(\xi_j,\tau) - P_x(\mu_j,\tau)\big)_{j=1}^M, \\ &\int_0^L Q(x,\tau)\,\mathrm{d}x, \big(Q_x(\alpha_k,\tau) - Q_x(\beta_k,\tau)\big)_{k=1}^N\Big). \end{aligned} \tag{9}$$

Proposition 4.1 (Necessary final-state observability) *Suppose that the control operator associated with (1) is L^2-admissible on $\mathcal{X}_*$. If the system is null controllable at time T, then there is $C_T > 0$ such that*

$$E_{P,Q}(T) \le C_T \int_0^T \|\mathcal{O}(P,Q)(t)\|^2_{\mathbb{C}^{M+N+1}} \, \mathrm{d}t \tag{10}$$

for every smooth time-reversed adjoint solution.

Proof Let $S(t)$ denote the homogeneous contraction semigroup on $\mathcal{X}_*$ and let B denote the (possibly unbounded) admissible control operator. The reachability operator at time T is

$$\mathcal{W}_T u = \int_0^T S(T-t)Bu(t)\,\mathrm{d}t, \qquad u \in L^2\big(0,T;\mathbb{C}^{M+N+1}\big).$$

Null controllability is the range inclusion $\operatorname{Ran} S(T) \subset \operatorname{Ran} \mathcal{W}_T$. For bounded operators between Hilbert spaces, the Douglas range-inclusion lemma is equivalent to the existence of $C_T > 0$ such that

$$\big\|S(T)^* z\big\|^2_{\mathcal{X}_*} \le C_T \, \big\|\mathcal{W}_T^* z\big\|^2_{L^2(0,T;\mathbb{C}^{M+N+1})} \qquad (z \in \mathcal{X}_*). \tag{11}$$

Admissibility makes $\mathcal{W}_T$ bounded, so the lemma applies. Directly from the definition of $\mathcal{W}_T$,

$$(\mathcal{W}_T^* z)(t) = B^* S(T-t)^* z.$$

Identity (8) identifies this vector with the patch and mean observations in (9). After the change of variable $\tau = T - t$, the adjoint evolves according to the time-reversed system and the left-hand side of (11) is its energy at $\tau = T$. This gives (10). Notice that the energy at T, rather than at 0, is essential: the damped shear semigroup is not invertible. This is the null-controllability form of the standard HUM duality argument [8]. □

5 High-frequency spectral obstruction

Set

$$q_n = \frac{n\pi}{L}, \qquad c = \sqrt{\frac{\kappa}{\rho}}, \qquad a = \frac{\lambda}{\gamma}, \qquad b = \frac{\kappa}{\gamma}.$$

For the homogeneous time-reversed adjoint, use

$$P(x,t) = P_n(t)\sin(q_n x), \qquad Q(x,t) = Q_n(t)\cos(q_n x).$$

These basis functions satisfy the boundary conditions and are orthogonal for different n. Since $(P_x + Q)_x = -q_n(q_n P_n + Q_n)\sin(q_n x)$ and $Q_{xx} = -q_n^2 Q_n \cos(q_n x)$, equality of the Fourier coefficients gives the modal equations

$$\rho\ddot{P}_n + \kappa q_n^2 P_n + \kappa q_n Q_n = 0, \qquad \gamma\dot{Q}_n + (\lambda q_n^2 + \kappa)Q_n + \kappa q_n P_n = 0. \tag{12}$$

For an exponential solution $(P_n, Q_n) = (A, B)e^{st}$, the amplitudes satisfy

$$\begin{pmatrix} \rho s^2 + \kappa q_n^2 & \kappa q_n \\ \kappa q_n & \gamma s + \lambda q_n^2 + \kappa \end{pmatrix} \begin{pmatrix} A \\ B \end{pmatrix} = 0.$$

A nonzero amplitude vector exists precisely when the determinant vanishes. After division by $\rho\gamma$ and cancellation of the two $\kappa^2 q_n^2$ terms, this determinant is

$$\mathcal{P}_n(s) = s^3 + (aq_n^2 + b)s^2 + c^2 q_n^2 s + c^2 a q_n^4 = 0. \tag{13}$$

Equivalently,

$$\mathcal{P}_n(s) = (s^2 + c^2 q_n^2)(s + aq_n^2) + bs^2. \tag{14}$$

Lemma 5.1 (Weakly damped wave branch) *For all sufficiently large n, (13) has a conjugate pair $s_n^{\pm}$ satisfying*

$$s_n^{\pm} = \pm icq_n + \frac{d_2^{\pm}}{q_n} + \frac{d_3}{q_n^2} + O(q_n^{-3}), \tag{15}$$

where

$$d_2^{\pm} = \mp i\frac{bc}{2a}, \qquad d_3 = -\frac{bc^2}{2a^2} = -\frac{\kappa^2\gamma}{2\rho\lambda^2} < 0.$$

In particular, $\operatorname{Re} s_n^{\pm} \to 0^-$ *at rate* q_n^{-2}.

Proof Write $s = q_n z$ and $\varepsilon = q_n^{-1}$. Dividing (13) by q_n^4 gives

$$F(z,\varepsilon) = a(z^2 + c^2) + \varepsilon z(z^2 + c^2) + b\varepsilon^2 z^2 = 0.$$

At $\varepsilon = 0$, the roots $z_0^{\pm} = \pm ic$ are simple. The analytic implicit-function theorem therefore gives analytic roots $z^{\pm}(\varepsilon)$ near $z_0^{\pm}$. Substitution of $z^{\pm} = z_0^{\pm} + d_2^{\pm}\varepsilon^2 + d_3\varepsilon^3 + O(\varepsilon^4)$ is justified because the coefficient of ε vanishes at $z = z_0^{\pm}$. To identify the next coefficients, first expand

$$\begin{aligned}
(z^{\pm})^2 + c^2 &= 2z_0^{\pm} d_2^{\pm}\varepsilon^2 + 2z_0^{\pm} d_3\varepsilon^3 + O(\varepsilon^4),\\
\varepsilon z^{\pm}\big((z^{\pm})^2 + c^2\big) &= 2(z_0^{\pm})^2 d_2^{\pm}\varepsilon^3 + O(\varepsilon^4),\\
b\varepsilon^2(z^{\pm})^2 &= b(z_0^{\pm})^2\varepsilon^2 + O(\varepsilon^4).
\end{aligned}$$

Comparison of the ε^2 and ε^3 coefficients now gives

$$2az_0^{\pm} d_2^{\pm} + b(z_0^{\pm})^2 = 0, \qquad 2az_0^{\pm} d_3 + 2(z_0^{\pm})^2 d_2^{\pm} = 0.$$

Because $z_0^{\pm} = \pm ic$, the first equation yields $d_2^{\pm} = -bz_0^{\pm}/(2a) = \mp ibc/(2a)$. Substitution in the second equation yields $d_3 = -bc^2/(2a^2)$, which is real and strictly negative. Finally, $s = q_n z^{\pm}(q_n^{-1})$ gives (15). Complex conjugacy follows because (13) has real coefficients. □

The q_n^{-2} real part is consistent with the sharp polynomial decay found for rotationally damped shear beams in [11, 15]. It is also the feature that prevents damping from removing the following observation defect.

Lemma 5.2 (Quantitative simultaneous recurrence of patch lengths) *Assume $M \geq 1$. For any fixed displacement-patch intervals (ξ_j, μ_j), $1 \leq j \leq M$, there are a constant $C_D > 0$ and a strictly increasing sequence (n_ℓ) such that*

$$\max_{1\leq j\leq M} \big|\cos(q_{n_\ell}\xi_j) - \cos(q_{n_\ell}\mu_j)\big| \leq C_D n_\ell^{-1/M}. \tag{16}$$

Proof Set $\theta_j = (\mu_j - \xi_j)/(2L)$ and fix an integer $Q \geq 2$. Consider the $Q^M + 1$ points

$$\big(\{r\theta_1\}, \dots, \{r\theta_M\}\big) \in [0,1)^M, \qquad 0 \leq r \leq Q^M,$$

where $\{\cdot\}$ denotes fractional part. Divide the unit cube into Q^M half-open cubes of side Q^{-1}. Two of the displayed points lie in the same small cube. Subtracting their indices produces an integer $1 \leq n \leq Q^M$ such that

$$\max_{1 \leq j \leq M} \big\|n\theta_j\big\|_{\mathbb{Z}} \leq Q^{-1} \leq n^{-1/M}.$$

Letting $Q \to \infty$ produces infinitely many distinct such n, unless one fixed n recurs for arbitrarily large Q. In the latter case $n\theta_j \in \mathbb{Z}$ for every j, and all positive multiples of n give exact simultaneous recurrence. Thus in either case there is a strictly increasing sequence (n_ℓ) satisfying the displayed estimate.

It remains to translate approximation of the patch lengths into approximation of the observation coefficients. The identity

$$\cos(q_n\xi_j) - \cos(q_n\mu_j) = 2\sin\!\left(\frac{q_n(\xi_j + \mu_j)}{2}\right)\sin\!\left(\frac{q_n(\mu_j - \xi_j)}{2}\right)$$

and the equality $q_n(\mu_j - \xi_j)/2 = \pi n\theta_j$ give

$$\big|\cos(q_n\xi_j) - \cos(q_n\mu_j)\big| \leq 2\pi\,\big\|n\theta_j\big\|_{\mathbb{Z}}.$$

This proves (16), with $C_D = 2\pi$. See [2, 4] for this approximation principle in point-actuator problems. □

For $K \geq 1$, let $\mathcal{X}_K \subset \mathcal{X}_*$ be the spectral Galerkin space generated by the sine–cosine modes with $1 \leq n \leq K$. Denote by $\mathcal{C}_K(T)$ the smallest constant in (10) when the adjoint data are restricted to $\mathcal{X}_K$, with the convention $\mathcal{C}_K(T) = +\infty$ if the finite-dimensional inequality fails.

Theorem 5.3 (Multi-patch obstruction and cost blow-up) *Fix $M, N < \infty$, arbitrary patch endpoints, and $T > 0$. Even when the uniform input h is allowed, no L^2-admissible realization of (1)–(2) is null controllable in the natural zero-mean energy space $\mathcal{X}_*$ at time T.*

More precisely, set

$$\sigma_M = \begin{cases} 1, & M = 0, \\ 1/M, & M \geq 1. \end{cases}$$

There are $c_T > 0$ and a strictly increasing sequence (n_ℓ) such that

$$\mathcal{C}_{n_\ell}(T) \geq c_T\, n_\ell^{2\sigma_M}. \tag{17}$$

Consequently, the worst-case norm of a least-energy control for the n_ℓ-mode Galerkin system is at least $c_T^{1/2} n_\ell^{\sigma_M}$; it is understood to be infinite when that truncation is not controllable.

Proof Let $s_n = s_n^+$ be the root from Lemma 5.1. Define the smooth time-reversed adjoint mode

$$P^{(n)}(x,t) = q_n^{-1} e^{s_n t}\sin(q_n x), \tag{18}$$

$$Q^{(n)}(x,t) = R_n e^{s_n t}\cos(q_n x), \qquad R_n = -\frac{s_n^2 + c^2 q_n^2}{c^2 q_n^2}. \tag{19}$$

Equations (12) follow from (13), so this is an exact adjoint solution. Indeed, the first modal equation reduces to

$$\frac{s_n^2 + c^2 q_n^2}{q_n} + c^2 q_n R_n = 0,$$

which is the definition of R_n, and the second one then follows from the zero determinant (13). Using $s_n = icq_n + d_2^+/q_n + d_3/q_n^2 + O(q_n^{-3})$ gives

$$s_n^2 + c^2 q_n^2 = 2icd_2^+ + O(q_n^{-1}) = \frac{bc^2}{a} + O(q_n^{-1}).$$

Consequently,

$$R_n = -\frac{b}{a} q_n^{-2} + O(q_n^{-3}), \qquad q_n R_n = -\frac{b}{a} q_n^{-1} + O(q_n^{-2}). \tag{20}$$

The energy is obtained by integrating $|\sin(q_n x)|^2 = |\cos(q_n x)|^2 = L/2$. Hence

$$\begin{aligned} E_{P^{(n)},Q^{(n)}}(0) &= \frac{L}{4}\left(\rho\left|\frac{s_n}{q_n}\right|^2 + \lambda q_n^2 |R_n|^2 + \kappa|1+R_n|^2\right) \\ &\longrightarrow \frac{L}{4}(\rho c^2 + \kappa) = \frac{\kappa L}{2} > 0, \end{aligned}$$

because $s_n/q_n \to ic$, $q_n R_n \to 0$, and $R_n \to 0$. Thus the modes can be multiplied by normalization constants that remain bounded above and below. We perform this normalization and henceforth assume that their initial energy is one.

If $M \geq 1$, choose the subsequence from Lemma 5.2. For the jth displacement patch,

$$\begin{aligned} &P_x^{(n_\ell)}(\xi_j, t) - P_x^{(n_\ell)}(\mu_j, t) \\ &\quad = e^{s_{n_\ell} t}\big(\cos(q_{n_\ell}\xi_j) - \cos(q_{n_\ell}\mu_j)\big). \end{aligned}$$

Since $\operatorname{Re} s_n < 0$ for all sufficiently large n,

$$J_n(T) := \int_0^T e^{2t \operatorname{Re} s_n}\,\mathrm{d}t \leq T.$$

Therefore each squared displacement-observation norm is bounded by $TC_D^2 n_\ell^{-2/M}$. If $M = 0$, these observations are absent. In that case take $n_\ell = \ell$ (after discarding the finitely many indices not covered by Lemma 5.1). For every rotation patch, (20) gives, uniformly in its endpoints,

$$\left|Q_x^{(n)}(\alpha_k, t) - Q_x^{(n)}(\beta_k, t)\right| \leq 2q_n|R_n|e^{\operatorname{Re} s_n t} = O(n^{-1}).$$

Its squared $L^2(0,T)$ norm is therefore $O(n^{-2})$. The number of rotation patches is fixed, so summing these bounds only changes the constant. The uniform-channel observation vanishes exactly because $\int_0^L \cos(q_n x)\,\mathrm{d}x = 0$. Combining all channels, and recalling that $n^{-2} \leq n^{-2/M}$ when $M \geq 1$, gives

$$\int_0^T \left\|\mathcal{O}(P^{(n_\ell)}, Q^{(n_\ell)})(t)\right\|^2 \,\mathrm{d}t \leq C_T n_\ell^{-2\sigma_M}. \tag{21}$$

On the other hand,

$$E_{P^{(n_\ell)},Q^{(n_\ell)}}(T) = e^{2T \operatorname{Re} s_{n_\ell}} \longrightarrow 1.$$

In particular, this final energy is at least $1/2$ for all sufficiently large ℓ. The right-hand side of (21) tends to zero, whereas the left-hand side of the necessary inequality (10) does not. This contradiction proves the infinite-dimensional claim.

For the quantitative statement, the test mode belongs to $\mathcal{X}_{n_\ell}$. By the definition of the best Galerkin observability constant,

$$\mathcal{C}_{n_\ell}(T) \geq \frac{E_{P^{(n_\ell)},Q^{(n_\ell)}}(T)}{\displaystyle\int_0^T \left\| \mathcal{O}(P^{(n_\ell)}, Q^{(n_\ell)})(t) \right\|^2 \, \mathrm{d}t} \geq c_T n_\ell^{2\sigma_M},$$

which is (17). In a controllable finite-dimensional truncation, the optimal observability constant is the square of the operator norm that maps an initial state to its minimum-L^2 null control (equivalently, it is determined by the inverse reachability Gramian). Taking square roots gives the asserted $n_\ell^{\sigma_M}$ lower bound. If the truncation is not controllable, both costs are infinite by convention, so the conclusion still holds. □

Corollary 5.4 *Neither adding more patches nor adding a spatially uniform rotation actuator repairs natural-energy null controllability. Irrational patch lengths may prevent an individual coefficient from vanishing exactly, but no finite placement supplies the required uniform lower bound. For the original two-patch architecture ($M = 1$ in the displacement equation), the Galerkin observability constants grow at least quadratically and the least-control norms at least linearly along a subsequence.*

6 Structure-preserving approximation and numerical experiments

The numerical section of [3] combines a stable spatial discretization, a discrete energy estimate, and plots of pointwise traces and energy. We follow that organization, but use a Fourier–Galerkin method because the obstruction in Theorem 5.3 is spectral. In addition to time-domain traces, we compute quantities that directly test Lemmas 5.1 and 5.2.

6.1 Fourier–Galerkin system and time discretization

For the homogeneous problem, truncate the expansion at mode K:

$$w_K(x,t) = \sum_{n=1}^{K} W_n(t) \sin(q_n x), \qquad \varphi_K(x,t) = \sum_{n=1}^{K} \Phi_n(t) \cos(q_n x), \qquad V_n = \dot{W}_n.$$

The coefficient vector $X_n = (W_n, V_n, \Phi_n)^\top$ satisfies

$$\dot{X}_n = A_n X_n, \qquad A_n = \begin{pmatrix} 0 & 1 & 0 \\ -c^2 q_n^2 & 0 & -c^2 q_n \\ -b q_n & 0 & -(a q_n^2 + b) \end{pmatrix}. \tag{22}$$

Let $t_m = m\Delta t$ and write $Z^{m+1/2} = (Z^{m+1} + Z^m)/2$. We use the implicit-midpoint scheme

$$\begin{cases} \dfrac{W_n^{m+1} - W_n^m}{\Delta t} = V_n^{m+1/2}, \\ \rho \dfrac{V_n^{m+1} - V_n^m}{\Delta t} + \kappa q_n^2 W_n^{m+1/2} + \kappa q_n \Phi_n^{m+1/2} = 0, \\ \gamma \dfrac{\Phi_n^{m+1} - \Phi_n^m}{\Delta t} + (\lambda q_n^2 + \kappa)\Phi_n^{m+1/2} + \kappa q_n W_n^{m+1/2} = 0. \end{cases} \tag{23}$$

Equivalently, $X_n^{m+1} = (I - \Delta t A_n/2)^{-1}(I + \Delta t A_n/2)X_n^m$. The inverse exists because every eigenvalue of A_n lies in the closed left half-plane, whereas $2/\Delta t > 0$.

Define the discrete energy

$$E_K^m = \frac{L}{4} \sum_{n=1}^{K} \left(\rho |V_n^m|^2 + \lambda q_n^2 |\Phi_n^m|^2 + \kappa |q_n W_n^m + \Phi_n^m|^2 \right). \tag{24}$$

Proposition 6.1 (Exact discrete dissipation law) *Every solution of* (23) *satisfies*

$$E_K^{m+1} - E_K^m = -\frac{\gamma L}{2\Delta t} \sum_{n=1}^{K} |\Phi_n^{m+1} - \Phi_n^m|^2 \le 0. \tag{25}$$

Proof Fix n and set $\Delta W_n = W_n^{m+1} - W_n^m$, with analogous notation for V_n and Φ_n. Multiply the second equation in (23) by $\overline{\Delta W_n} = \Delta t\, \overline{V_n^{m+1/2}}$, multiply the third by $\overline{\Delta \Phi_n}$, add the results, and take real parts. If $S_n^m = q_n W_n^m + \Phi_n^m$, the stiffness terms combine as

$$\begin{aligned} &\kappa q_n^2 \operatorname{Re}(W_n^{m+1/2}\overline{\Delta W_n}) + \kappa q_n \operatorname{Re}(\Phi_n^{m+1/2}\overline{\Delta W_n}) \\ &\quad + \kappa q_n \operatorname{Re}(W_n^{m+1/2}\overline{\Delta \Phi_n}) + \kappa \operatorname{Re}(\Phi_n^{m+1/2}\overline{\Delta \Phi_n}) \\ &= \kappa \operatorname{Re}(S_n^{m+1/2}\overline{\Delta S_n}). \end{aligned}$$

For any complex numbers z_0, z_1,

$$\operatorname{Re}\left(\frac{z_1 + z_0}{2} \overline{(z_1 - z_0)} \right) = \frac{1}{2}(|z_1|^2 - |z_0|^2).$$

Applying this identity to V_n, Φ_n, and S_n yields

$$\begin{aligned} \frac{1}{2}\Big[&\rho(|V_n^{m+1}|^2 - |V_n^m|^2) + \lambda q_n^2 (|\Phi_n^{m+1}|^2 - |\Phi_n^m|^2) \\ &+ \kappa(|S_n^{m+1}|^2 - |S_n^m|^2) \Big] + \frac{\gamma}{\Delta t} |\Delta \Phi_n|^2 = 0. \end{aligned}$$

Multiply by $L/2$ and sum over $1 \le n \le K$. The bracket becomes $E_K^{m+1} - E_K^m$, proving (25). □

Thus the method has no artificial energy growth. Unlike backward Euler, the midpoint rule does not add numerical damping to the conservative part of the wave branch; this matters when the physical real parts are only $O(q_n^{-2})$.

6.2 Experimental setting

All experiments use

$$L = \rho = \lambda = \kappa = \gamma = 1, \qquad a = b = c = 1. \tag{26}$$

For the time-domain experiment, $K = 6$, $T = 80$, and $\Delta t = 5 \times 10^{-3}$. The initial modal coefficients are

$$W_1^0 = 1, \qquad W_3^0 = \frac{1}{3}, \qquad V_n^0 = \Phi_n^0 = 0,$$

with all other $W_n^0 = 0$. The factor $1/3$ gives the first and third displacement modes equal initial shear energy. We record w_K and φ_K at $x = 0.25, 0.50, 0.75$.

For the spectral experiment, roots of (13) are computed for $1 \le n \le 1500$ and the control horizon is $T = 2$. The first displacement architecture is

$$\mathcal{A}_1 = \left\{ \left(0.17, 0.17 + \frac{\sqrt{2}}{10} \right) \right\},$$

and the second is

$$\mathcal{A}_2 = \mathcal{A}_1 \cup \left\{ \left(0.43, 0.43 + \frac{\sqrt{3}}{11} \right) \right\}.$$

Both use one rotation patch $(0.31, 0.67)$. The irrational lengths avoid a deliberately resonant example; Lemma 5.2 still predicts near-recurrence. For the normalized wave mode, define the computable quotient

$$\begin{aligned} \mathcal{Q}_n(T) &= \frac{E_n(T)}{J_n(T) D_n}, \\ D_n &:= \sum_{(\xi,\mu)\in\mathcal{A}} |\cos(q_n \xi) - \cos(q_n \mu)|^2 \\ &\quad + q_n^2 |R_n|^2 |\sin(0.31 q_n) - \sin(0.67 q_n)|^2, \end{aligned} \tag{27}$$

where $J_n(T) = \int_0^T e^{2t \operatorname{Re} s_n^+} \, \mathrm{d}t$. For $n \le K$, $\mathcal{Q}_n(T)$ is a lower bound for $\mathcal{C}_K(T)$.

6.3 Results and interpretation

Figure 1(a)–(b) displays damped oscillations. The rotation trace at $x = 0.5$ is zero because the chosen initial data contain only odd cosine modes. Panel (c) confirms monotonicity: the normalized energy decreases from 1 to approximately 0.208 over the plotted interval. The maximum positive energy increment was -5.27×10^{-9} (that is, every increment was negative), and the maximum residual in (25) was 2.53×10^{-15}. Panel (d) shows the central nonuniformity: the $n = 1$ wave mode decays substantially on $[0, 80]$, whereas the $n = 12$ mode loses very little energy because $\operatorname{Re} s_n^+ = O(-n^{-2})$.

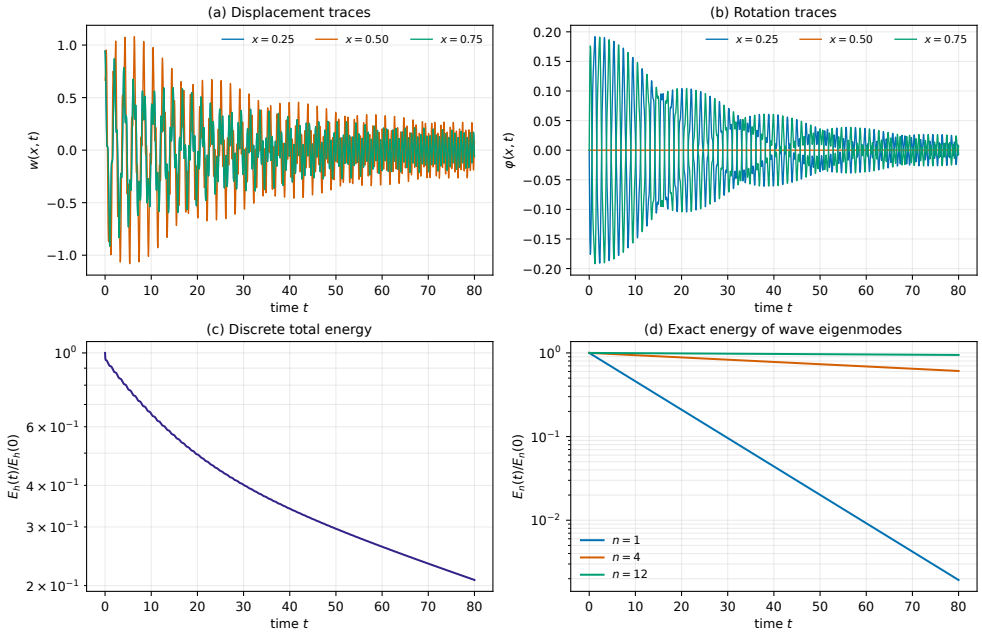


Fig. 1 Time-domain Fourier–Galerkin experiment for (26). Panels (a)–(b) show displacement and rotation traces; panel (c) shows the monotone discrete energy from (24); panel (d) compares exact normalized energies of three wave eigenmodes

Table 1 Numerical verification of the asymptotic constants for $a = b = c = 1$. The theoretical limits are $1/2$ and 1, respectively

n	$-q_n^2 \operatorname{Re} s_n^+$	$q_n^2 \lvert R_n \rvert$
5	0.4940016	0.9939835
10	0.4984853	0.9984841
25	0.4997570	0.9997569
50	0.4999392	0.9999392
100	0.4999848	0.9999848
200	0.4999959	0.9999962

Panels (a)–(b) of Figure 2 and Table 1 numerically confirm

$$-q_n^2 \operatorname{Re} s_n^+ \longrightarrow \frac{1}{2}, \qquad q_n^2 |R_n| \longrightarrow 1,$$

which are the constants obtained from (15) and (20) when all physical coefficients equal one. Panel (c) shows sharp, sparse peaks rather than monotone modal growth; this is the numerical signature of Diophantine recurrence. Panel (d) takes running maxima,

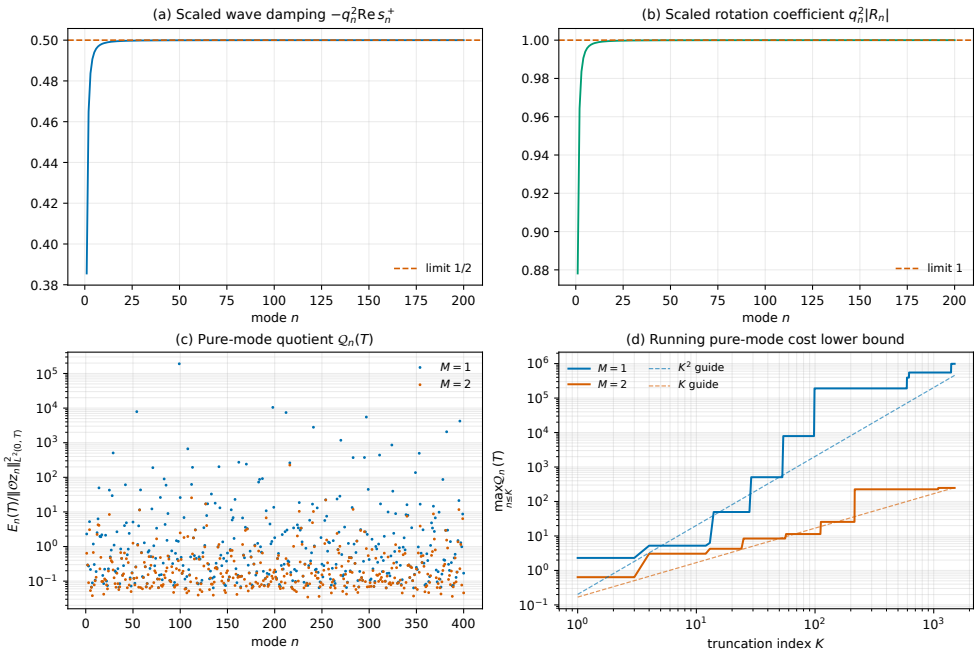


Fig. 2 Spectral and observability diagnostics for $T = 2$. Panels (a)–(b) verify the asymptotic constants. Panel (c) shows the irregular pure-mode quotients (27). Panel (d) shows their running maxima; the dashed K^2 and K curves indicate the subsequential powers predicted for $M = 1$ and $M = 2$ and are guides, not fitted global asymptotics

the quantity relevant to Galerkin observability. For $M = 1$ it reaches 9.86×10^5 by $K = 1500$, while for $M = 2$ it reaches 2.47×10^2. The difference is consistent with the exponent $2/M$ in Theorem 5.3: adding a patch can reduce the rate of cost deterioration, but no finite M makes the family uniformly observable.

These computations illustrate the proof but do not replace it. In particular, a finite scan cannot establish an infinite subsequence, and the location of individual peaks depends on the chosen patch lengths. The source code and CSV tables underlying the figures and table are provided in Online Resource 1.

7 Relation with the literature

The result above uses the generator framework of Ramos et al. [12], but their resolvent construction only proves lack of exponential stability. It does not imply failure of null controllability, nor does it quantify Galerkin control costs. Those conclusions require the adjoint eigenmodes and simultaneous recurrence developed here.

- Lo and Tatar [9, 10] study two-layer Timoshenko beams with an additional variable describing interfacial slip. In [9], viscoelastic memory on the effective rotation gives exponential decay under the stated relaxation-kernel and coefficient restrictions. In [10], exponential decay follows either from transverse friction

(together with the structural slip damping) or from two memory terms under a small-relaxation-mass condition. These theorems identify successful passive damping designs, but they neither assert null controllability nor furnish the patch-observability inequality (10). Thus they complement, rather than contradict, Theorem 5.3.

- For a Rayleigh beam with a piezoelectric actuator, [2] proves that the controllable space depends on both actuator arithmetic and control regularity. Its L^2 result is posed in a substantially smoother Sobolev space and requires a sufficiently long control time. The same paper proves non-controllability for rougher data and in short time. These conclusions rule out transferring an "all energy data, all $T > 0$" statement to the present model.
- The Timoshenko system in [14] is fully hyperbolic, has dynamic boundary variables, and is controlled at the boundary. Its HUM observation and state space are therefore different from the interior point-moment observations in (9).
- Boundary and partial controllability of Mindlin–Timoshenko systems uses non-compact boundary traces and spectral gap estimates [1]. Such results do not transfer to finitely many interior endpoint moments, precisely because of Lemma 5.2.
- The thermoelastic shear model in [3] contains an additional heat equation and a different dissipation mechanism. Its exponential stability result cannot be used as a spectral estimate for (1). Its treatment of a Neumann mean mode does, however, reinforce the necessity of isolating invariant averages.
- For one-dimensional wave–heat cascades, [7] obtains a sharp hyperbolic control time and weighted reachable spaces through a Riesz-basis/Ingham–Müntz analysis. This supports a future search for a weighted controllability space for the shear system, but it cannot supply natural-energy observability contradicted by Theorem 5.3.

Taken together, these comparisons show that the obstruction is not a formal consequence of the lack of exponential stability alone. It results from the specific combination of a weakly damped wave branch, finite endpoint-moment observations, and simultaneous arithmetic recurrence. None of the cited positive results supplies the uniform natural-energy observability inequality ruled out by Theorem 5.3.

8 Outlook

The negative result leaves several mathematically meaningful problems.

(a) Determine the sharp Sobolev scale in which the loss of the patch coefficients is compensated and null controllability may hold.
(b) Study approximate controllability under explicit non-resonance conditions on all patch lengths and midpoints.
(c) Use boundary traces, which are non-compact, or an infinite-dimensional distributed control in place of the finite endpoint moments. A uniform mean channel alone is insufficient by Theorem 5.3.

(d) Motivated by the successful damping mechanisms in [9, 10], determine whether adding a genuine memory variable or transverse distributed friction changes the sharp weighted controllability space. Exponential stability by itself is not enough for null controllability, so this question still requires an independent admissibility and observability analysis.
(e) Establish admissibility and hidden regularity for every chosen slope observation before attempting a positive HUM theorem.

9 Conclusion

Two independent mechanisms invalidate L^2-null controllability of the rotationally damped shear beam in its natural energy space. Pure endpoint moments miss the rotation mean; a uniform input repairs that scalar defect. Nevertheless, on the zero-mean invariant subspace, weakly damped wave modes are arbitrarily poorly observed by every finite family of patches. The resulting Galerkin cost blow-up is at least polynomial with an exponent determined by the number of displacement patches. Thus neither irrational placement nor finitely many additional patches can produce natural-energy null controllability. The structure-preserving Fourier–Galerkin experiments independently reproduce the weak $O(q_n^{-2})$ damping, verify the exact discrete energy law to roundoff accuracy, and display the predicted growth of the truncated observability cost. A positive theorem must instead change the state regularity, the controllability notion, or the actuator class.

Supplementary information

Online Resource 1 contains the reproducibility code and comma-separated-value data underlying Figs. 1–2 and Table 1.

Acknowledgements

The authors gratefully acknowledge the University of Wollongong in Dubai for its support.

Statements and Declarations

Funding

This work was supported by the University of Wollongong in Dubai through Internal Project RY24005.

Competing interests

The authors have no relevant financial or non-financial interests to disclose.

Data availability

The numerical data supporting the findings of this study are provided in Online Resource 1 with the submission.

Code availability

The code used to generate the numerical data and figures is provided in Online Resource 1 with the submission.

Author contributions

All authors contributed to the conception and design of the study, the mathematical analysis, and preparation of the manuscript. All authors read and approved the final manuscript.

Ethics approval and consent to participate

Not applicable.

Consent for publication

Not applicable.

Materials availability

Not applicable.

References

[1] Araruna FD, Zuazua E (2008) Controllability of the Kirchhoff system for beams as a limit of the Mindlin–Timoshenko system. SIAM Journal on Control and Optimization 47:1909–1938. https://doi.org/10.1137/060659934

[2] Bai Y, Prieur C, Wang Z (2024) Exact controllability for a Rayleigh beam with piezoelectric actuator. Systems & Control Letters 186:105759. https://doi.org/10.1016/j.sysconle.2024.105759

[3] Benmoussa A, Fareh A, Messaoudi SA, et al (2022) Well posedness and exponential stability of a thermoelastic shear beam model. Research Square preprint, https://doi.org/10.21203/rs.3.rs-2203876/v1

[4] Cassels JWS (1957) An Introduction to Diophantine Approximation. Cambridge University Press, Cambridge

[5] Crawley EF, de Luis J (1987) Use of piezoelectric actuators as elements of intelligent structures. AIAA Journal 25:1373–1385. https://doi.org/10.2514/3.9792

[6] Crépeau E, Prieur C (2006) Control of a clamped-free beam by a piezoelectric actuator. ESAIM: Control, Optimisation and Calculus of Variations 12:545–563. https://doi.org/10.1051/cocv:2006008

[7] Lhachemi H, Prieur C, Trélat E (2026) Controllability of wave–heat and heat–wave cascades. arXiv:2601.18212, https://doi.org/10.48550/arXiv.2601.18212

[8] Lions JL (1988) Exact controllability, stabilization and perturbations for distributed systems. SIAM Review 30:1–68. https://doi.org/10.1137/1030001

[9] Lo A, Tatar Ne (2015) Stabilization of laminated beams with interfacial slip. Electronic Journal of Differential Equations 2015(129):1–14. URL https://ejde.math.txstate.edu/Volumes/2015/129/lo.pdf

[10] Lo A, Tatar Ne (2016) Exponential stabilization of a structure with interfacial slip. Discrete and Continuous Dynamical Systems 36(11):6285–6306. https://doi.org/10.3934/dcds.2016073

[11] Nonato CNS, Júnior D, Miranda LGR, et al (2026) On the optimal polynomial decay of shear beams under rotational damping. Annali dell'Università di Ferrara 72. https://doi.org/10.1007/s11565-026-00662-z, article 39

[12] Ramos AJA, Almeida Júnior DS, Freitas MM, et al (2022) About well-posedness and lack of exponential stability of shear beam models. Annali dell'Università di Ferrara 68:129–136. https://doi.org/10.1007/s11565-022-00391-z

[13] Tucsnak M (1996) Regularity and exact controllability for a beam with piezoelectric actuator. SIAM Journal on Control and Optimization 34:922–930. https://doi.org/10.1137/S0363012994265468

[14] Zhang CG, Hu HX (2007) Exact controllability of a Timoshenko beam with dynamical boundary. Journal of Mathematics of Kyoto University 47:643–655. https://doi.org/10.1215/kjm/1250281029

[15] Zhang XF, Cao TC, Zhao ZX, et al (2026) Optimal polynomial decay rate for a damped shear beam model. Applied Mathematics Letters 177:109877. https://doi.org/10.1016/j.aml.2026.109877